2011

The analytical evolution of NLS solitons due to the numerical discretization error

S. M. Hoseini
University Rafsanjan

Timothy R. Marchant
University of Wollongong, tim@uow.edu.au

The analytical evolution of NLS solitons due to the numerical discretization error

Abstract

Soliton perturbation theory is used to obtain analytical solutions describing solitary wave tails or shelves, due to numerical discretization error, for soliton solutions of the nonlinear Schr¨odinger equation. Two important implicit numerical schemes for the nonlinear Schr¨odinger equation, with second-order temporal and spatial discretization errors, are considered. These are the Crank– Nicolson scheme and a scheme, due to Taha [1], based on the inverse scattering transform. The first-order correction for the solitary wave tail, or shelf, is in integral form and an explicit expression is found for large time. The shelf decays slowly, at a rate of t−12 , which is characteristic of the nonlinear Schr¨odinger equation. Singularity theory, usually used for combustion problems, is applied to the explicit large-time expression for the solitary wave tail. Analytical results are then obtained, such as the parameter regions in which qualitatively different types of solitary wave tails occur, the location of zeros and the location and amplitude of peaks. It is found that three different types of tail occur for the Crank–Nicolson and Taha schemes and that the Taha scheme exhibits some unusual symmetry properties, as the tails for left and right moving solitary waves are different. Optimal choices of the discretization parameters for the numerical schemes are also found, whichminimize the amplitude of the solitary wave tail. The analytical solutions are compared with numerical simulations, and an excellent comparison is found.

Disciplines

Physical Sciences and Mathematics

Publication Details

Hoseini, S. & Marchant, T. R. (2011). The analytical evolution of NLS solitons due to the numerical discretization error. Journal of Physics A: Mathematical and Theoretical, 44 (50), 1-17.

The analytical evolution of NLS solitons, due to numerical discretization error

S.M.Hoseini[1] **and T.R. Marchant**[2]

[1] Mathematics Department, Vali-E-Asr University,
Rafsanjan, Iran.

E-mail: hoseini@uow.edu.au
[2] School of Mathematics and Applied Statistics,
The University of Wollongong,
Wollongong, 2522, N.S.W., Australia.

E-mail: tim_marchant@uow.edu.au

PACS numbers: 05.45Yv, 02.70Bf, 02.30Ik

Abstract. Soliton perturbation theory is used to obtain analytical solutions describing solitary wave tails or shelves, due to numerical discretization error, for soliton solutions of the nonlinear Schrödinger equation. Two important implicit numerical schemes for the nonlinear Schrödinger equation, with second-order temporal and spatial discretization errors, are considered. These are the Crank-Nicolson scheme and a scheme, due to Taha [1], based on the Inverse Scattering Transform. The first-order correction for the solitary wave tail, or shelf, is in integral form and an explicit expression is found, for large time. The shelf decays slowly, at a rate of $t^{-\frac{1}{2}}$, which is characteristic of the nonlinear Schrödinger equation. Singularity theory, usually used for combustion problems, is applied to the explicit large time expression for the solitary wave tail. Analytical results are then obtained, such as the parameter regions in which qualitatively different types of solitary wave tails occur, the location of zeros and the location and amplitude of peaks. It is found that three different types of tail occur for the Crank-Nicolson and Taha schemes and that the Taha scheme exhibits some unusual symmetry properties, as the tails for left and right moving solitary waves are different. Optimal choices of the discretization parameters for the numerical schemes are also found, which minimize the amplitude of the solitary wave tail. The analytical solutions are compared with numerical simulations and an excellent comparison is found.

1. Introduction

One of the most important model equations in nonlinear science is the nonlinear Schrödinger (NLS) equation,

$$i\eta_t + \eta_{xx} + \eta|\eta|^2 = 0. \tag{1}$$

Physically, the NLS equation describes the modulation of weakly-nonlinear wavetrains in deep water. [2] showed that an uniform wavetrain is unstable to longwave perturbations. [3] and [4] present a historical overview of fluid mechanics applications of the NLS equation and its physical origins. In the optical context, the NLS equation was derived by [5]. It also describes the evolution of the slowly varying envelope of an optical pulse. Derived asymptotically from Maxwell's equations, it assumes slow variation in the carrier frequency and the Kerr dependence (where the nonlinear refractive index $n = n_0 + n_1|\eta|^2$). The NLS equation is central to understanding soliton propagation in optical fibres, which is of critical importance to the field of fibre-based telecommunications, see [6].

A powerful analytical solution technique is direct soliton perturbation theory. This requires that the complete set of eigenfunctions for the linearized problem, related to the nonlinear wave equation, be determined. [7] constructed this set for a large class of integrable nonlinear wave equations such as the Korteweg-de Vries (KdV), NLS and modified KdV equations. The same procedure can be exploited to find the eigenstates of the adjoint linearization operator. He found that the eigenfunctions for these hierarchies are the squared Jost solutions. [8] developed direct soliton perturbation theory for the derivative NLS and the modified NLS equations. Using the similarity between the KdV and derivative NLS hierarchies they showed that the eigenfunctions for the linearized derivative NLS equation are the derivatives of the squared Jost solutions. This is in contrast to the counterpart for NLS, Hirota and mKdV hierarchies, where the eigenfunctions are just the squared Jost solutions. Suppressing the secular terms, they also found the slow evolution of soliton parameters and the perturbation-induced radiation.

[9] examined bright solitary wave interaction for a focusing version of the higher-order Hirota equation. A family of higher-order embedded solitons was found by using an asymptotic transformation. When embedded solitons do not exist, soliton perturbation theory was used to determine the details of a single evolving solitary wave, to first-order. In particular, an integral expression was found for the first-order correction to the solitary wave profile. They also asymptotically analysed the integral expression to derive an analytical form for the tail of the solitary wave. It was shown that for the right-moving solitary wave, a steady-state tail forms, while for the left-moving wave, some transients propagate on the steady-state tail.

[10] considered solitary wave interaction for a higher-order NLS equation, via an asymptotic transformation. The higher-order terms corresponded to a generalised version of the next even member of the NLS integrable hierarchy. They found an algebraic relationship, which when satisfied, results in an elastic solitary wave collision. When the collision is inelastic they found that a slowly decaying (like $t^{-\frac{1}{2}}$) bed, or shelf, of radiation forms under the waves. [11] considered the evolution of a general initial pulse, to the

NLS soliton solution. Using an averaged Lagrangian approach, they derived approximate evolution equations for the NLS soliton parameters and the radiation. In particular, the evolution equations described the interaction between the pulse and the bed of radiation, which again is slowly decaying.

[12] considered a perturbed NLS equation, where the higher-order terms are from the next even member of the NLS integrable hierarchy. Soliton perturbation theory was used to find an explicit expression for the solitary wave tail, at large time. Analytical results were then obtained, for the parameter regions in which qualitatively different types of tail occur, and the location of zeros and peaks in the tail. Two applications were examined in detail, the the near-continuum limit of a discrete NLS equation and the leading order discretization errors for an explicit NLS numerical scheme. It was shown that three different types of tail could occur for the evolution of a discrete soliton while only one type of tail occurred for the numerically evolving soliton.

[13] performed benchmarking studies on a wide range of NLS numerical schemes. These included explicit and implicit finite-difference schemes and finite Fourier transform methods. They performed numerical simulations of one and two-soliton solutions and found that finite Fourier methods and the Ablowitz and Ladik finite-difference scheme, derived from Inverse Scattering Theory (IST), proved to be most efficient. [1] derived a new IST based finite-difference scheme for the NLS equation, termed here the Taha scheme, which proved competitive with the Ablowitz-Ladik finite-difference scheme, for numerical simulations of the one-soliton solution. The Taha scheme is superior to other numerical schemes for solitons with small amplitudes but the Ablowitz-Ladik scheme was slightly faster, for large amplitude waves.

In this paper soliton perturbation theory is used to describe the evolution, due to numerical discretization error, of NLS solitons and the associated tails or shelves which form during this evolution. In §2 the Crank-Nicolson (CN) and Taha numerical schemes are presented and the terms contributing to the leading-order discretization error, are found. In §3 soliton perturbation theory is used to derive the details of an evolving solitary wave. The first-order correction to the solitary wave is found in integral form and an explicit expression, for large time, is derived. The large-time solution is investigated analytically using singularity theory, a technique usually applied to combustion problems. In §4 analytical and numerical results are presented for the solitary wave tails formed by evolution, due to the numerical discretization errors of CN and Taha schemes. The parameter space in which qualitatively different types of solitary wave tails occur is found and some unusual symmetry properties of the resultant solitary wave tail, for the Taha scheme are described. Also the parameter choices, which give a solitary wave tail of minimum amplitude, are found. These represent an optimal choice of discretization parameters for the CN and Taha numerical schemes, for a given NLS soliton.

2. Discretisation errors for the numerical schemes

The CN finite-difference scheme for NLS equation is

$$i(\eta_m^{n+1}-\eta_m^n)+\Delta t|\eta_m^{n+1}|^2\eta_m^{n+1}+\Delta t|\eta_m^n|^2\eta_m^n+\frac{s}{2}(\eta_{m+1}^n-2\eta_m^n \tag{2}$$
$$+\eta_{m-1}^n+\eta_{m+1}^{n+1}-2\eta_m^{n+1}+\eta_{m-1}^{n+1})=0,\quad \eta_m^n=\eta(m\Delta x,n\Delta t),\quad s=\frac{\Delta t}{\Delta x^2}.$$

This numerical scheme is unconditionally stable and the truncation error is $\mathrm{O}(\Delta x^2,\Delta t^2)$, see [13]. The solution of this scheme requires the solution of a tri-diagonal system of equations at each time step. This can be performed efficiently using the Thomas algorithm. As the coefficients of the tri-diagonal matrix are constant, the portion of the procedure that calculates the matrix coefficients, need only be performed once.

[1] proposed a new numerical scheme, termed here the Taha scheme, based on the IST. The form of the scheme is

$$\eta_m^{n+1}-\eta_m^n+(\eta_{m+2}^n+\eta_{m-2}^n)A^{(4)}-(\eta_{m+2}^{n+1}+\eta_{m-2}^{n+1})D^{(4)}+(\eta_{m+1}^n+\eta_{m-1}^n)A^{(2)}$$
$$-(\eta_{m+1}^{n+1}+\eta_{m-1}^{n+1})D^{(2)}+\eta_m^nA^{(0)}-\eta_m^{n+1}D^{(0)}+\Delta x^2[(\eta_{m+1}^n\eta_{m+2}^{n+1}\eta_{m+1}^{n+1^*}$$
$$+\eta_{m+1}^{n+1}\eta_m^{n+1^*}\eta_{m+1}^n+\eta_{m-1}^{n+1}\eta_{m-2}^n\eta_{m-1}^{n+1^*}+\frac{\eta_{m-1}^n}{2}(\eta_{m-1}^{n+1}\eta_m^{n+1^*}+\eta_{m-1}^n\eta_m^{n^*})$$
$$+\eta_m^{n+1}(\eta_{m-1}^n\eta_{m+1}^{n+1^*}+\eta_{m-2}^n\eta_m^{n+1^*})+\frac{\eta_m^n}{2}(\eta_{m+2}^{n+1}\eta_m^{n+1^*}+\eta_{m+1}^{n+1}\eta_{m-1}^{n+1^*}$$
$$+\eta_{m+2}^n\eta_m^{n^*}+\eta_{m+1}^n\eta_{m-1}^{n^*}))A^{(4)}-(\eta_{m+1}^n\eta_{m+1}^{n^*}\eta_{m+2}^{n+1}+\frac{\eta_{m+1}^{n+1}}{2}(\eta_m^{n+1^*}\eta_{m+1}^{n+1} \tag{3}$$
$$+\eta_m^{n^*}\eta_{m+1}^n)+\eta_{m-1}^{n+1}\eta_{m-1}^{n^*}\eta_{m-2}^n+\eta_{m-1}^n\eta_{m-1}^{n+1}\eta_m^{n^*}+\eta_m^n(\eta_m^{n^*}\eta_{m+2}^{n+1}+\eta_{m-1}^{n^*}\eta_{m+1}^{n+1})$$
$$+\frac{\eta_m^{n+1}}{2}(\eta_{m-1}^{n+1}\eta_{m+1}^{n+1^*}+\eta_{m-2}^{n+1}\eta_m^{n+1^*}+\eta_{m-1}^n\eta_{m+1}^{n^*}+\eta_{m-2}^n\eta_m^{n^*}))D^{(4)}$$
$$+(\frac{\eta_m^n}{2}(\eta_m^{n+1^*}\eta_{m+1}^{n+1}+\eta_m^{n^*}\eta_{m+1}^n)+\eta_m^{n+1}\eta_{m-1}^n\eta_m^{n+1^*})A^{(2)}$$
$$-(\frac{\eta_m^{n+1}}{2}(\eta_m^{n+1^*}\eta_{m-1}^{n+1}+\eta_m^{n^*}\eta_{m-1}^n)+\eta_m^n\eta_m^{n^*}\eta_{m+1}^{n+1})D^{(2)}]=0,\quad \text{where}$$
$$A^{(0)}=-D^{(0)}=\frac{5}{4}is,A^{(2)}=-D^{(2)}=-\frac{2}{3}is,A^{(4)}=-D^{(4)}=\frac{1}{24}is.$$

This scheme retains the integrable property of the NLS equation; this means that numerical soliton interactions are clean, with no dispersive radiation generated, as a result of the interaction. The truncation error of (3) is $\mathrm{O}(\Delta t^2,\Delta x^2,\Delta x\Delta t)$ and the scheme is unconditionally stable, see [13]. This scheme requires the solution of a penta-diagonal system of equations at each time step. A fast algorithm for this task is detailed in [14]. However, as the right hand side of the system of equations involves unknown values at the new time level, $t=(n+1)\Delta t$, iteration is also needed. This iteration procedure involves initially solving the matrix system using known values, from the old time level, $t=n\Delta t$ and then resolving, using the updated solution from the previous iteration.

Expanding the schemes (2) and (3) in a Taylor series, gives the perturbed NLS equation,

$$i\eta_t+\eta_{xx}+\eta|\eta|^2+\alpha H(\eta)=0,\quad \text{where}$$

$$
\begin{aligned}
H(\eta) &= c_1\eta_{4x} + c_2\eta^*_{4x}\eta^2 + c_3|\eta|^4\eta_{xx} + c_4\eta|\eta\eta_x|^2 + c_5\eta^3\eta^{*^2}_x + c_6\eta^3\eta^*\eta^*_{xx} \\
&+ c_7|\eta_x|^2\eta_{xx} + c_8\eta^*_{3x}\eta\eta_x + c_9\eta^*\eta_x\eta_{3x} + c_{10}\eta^*\eta^2_{xx} + c_{11}|\eta|^6\eta + c_{12}\eta^*_x\eta\eta_{3x} \\
&+ c_{13}|\eta|^2\eta^*\eta^2_x + c_{14}\eta^*_{xx}\eta^2_x + c_{15}\eta|\eta_{xx}|^2 + c_{16}\eta_{6x} + c_{17}|\eta|^2\eta_{4x} + c_{18}\eta^2\eta^*_{xx} \\
&+ c_{19}\eta^*\eta^2_x + c_{20}|\eta|^2\eta_{xx} + c_{21}\eta|\eta_x|^2 + ic_{22}|\eta|^2\eta_{3x} + ic_{23}\eta^2|\eta|^2\eta^*_x + ic_{24}|\eta|^4\eta_x \\
&+ ic_{25}\eta^*\eta_x\eta_{2x} + ic_{26}\eta\eta^*_x\eta_{2x} + ic_{27}\eta\eta_x\eta^*_{2x} + ic_{28}\eta^2\eta^*_{3x}, \quad \text{where} \quad \eta_{nx} = \frac{\partial^n\eta}{\partial x^n}.
\end{aligned} \tag{4}
$$

The perturbation terms H represent the leading order discretization errors, of the two numerical schemes. The higher-order coefficients c_j, for the schemes (2) and (3), are shown in table (1). Also note that $\alpha = \Delta t^2$ and the discretization ratio $\beta = \Delta x/\Delta t$. In the limit $\Delta x = \Delta t \to 0$ (4) reduces to the NLS equation and the discretization error (and the shelf) is zero.

c_j	CN	Taha	c_j	CN	Taha	c_j	CN	Taha
c_1	$\frac{1}{12}\beta^2$	0	c_{11}	$-\frac{2}{3}$	$-\frac{2}{3}$	c_{21}	0	$-\frac{1}{3}\beta^2$
c_2	$-\frac{1}{6}$	$-\frac{1}{6}$	c_{12}	-2	-2	c_{22}	0	$\frac{5}{12}\beta$
c_3	$-\frac{11}{3}$	$-\frac{53}{24}$	c_{13}	$-\frac{10}{3}$	$-\frac{10}{3}$	c_{23}	0	$\frac{11}{12}\beta$
c_4	-8	-8	c_{14}	$-\frac{5}{3}$	$-\frac{5}{3}$	c_{24}	0	$\frac{11}{12}\beta$
c_5	$-\frac{4}{3}$	$-\frac{4}{3}$	c_{15}	$-\frac{4}{3}$	$-\frac{33}{16}$	c_{25}	0	$-\frac{25}{24}\beta$
c_6	$-\frac{2}{3}$	$-\frac{17}{8}$	c_{16}	$-\frac{1}{12}$	$-\frac{1}{12}$	c_{26}	0	$-\frac{1}{24}\beta$
c_7	$-\frac{14}{3}$	$-\frac{14}{3}$	c_{17}	-1	-1	c_{27}	0	$\frac{5}{8}\beta$
c_8	$-\frac{2}{3}$	$-\frac{2}{3}$	c_{18}	0	$-\frac{1}{6}\beta^2$	c_{28}	0	$\frac{1}{24}\beta$
c_9	-2	-2	c_{19}	0	$-\frac{1}{2}\beta^2$			
c_{10}	$-\frac{5}{3}$	$-\frac{15}{16}$	c_{20}	0	$\frac{1}{3}\beta^2$			

Table 1. The coefficients of the perturbed NLS equation (4), corresponding to the leading-order discretization errors of the CN (2) and Taha (3) numerical schemes.

3. Soliton perturbation theory

In this section soliton perturbation theory, first developed by Yang and Kaup [15], is applied to find the first-order correction to the NLS solitary wave solution. This correction describes the evolution of NLS solitons, due to the perturbed NLS equation (4). For the coefficient choices in table 1 the evolution due to the leading order discretization errors of the CN and Taha numerical schemes is obtained.

3.1. Preliminaries

Soliton perturbation theory has been successfully applied to the NLS equation (1) by several authors. Here we review the important aspects of this theory, see Yang and Kaup [15] for more details. The unperturbed NLS equation (1) has the soliton solution

$$
\begin{aligned}
&\eta = \sqrt{2}\kappa e^{i\varphi}\,\mathrm{sech}\,\kappa\theta, \quad \text{where} \\
&\varphi = ax + (\kappa^2 - a^2)t + \varphi_0, \quad \theta = x - 2at - \theta_0,
\end{aligned} \tag{5}
$$

and the parameters κ, a, φ_0 and θ_0 are free. To model the perturbation, the solitary wave solution is defined as

$$\eta = e^{i(\delta+\frac{V}{2}\theta)}\omega(\theta,t,T;\alpha), \quad \text{where} \tag{6}$$
$$\delta = \int_0^t (\beta + \frac{1}{4}V^2)dt - \delta_0, \quad \theta = x - \int_0^t V dt - \theta_0.$$

Here the parameters V, β, δ_0 and θ_0 are considered as functions of the slow time $T = \alpha t$. Substituting (6) in (4) gives

$$i\omega_t + \omega_{\theta\theta} - \beta\omega + \omega|\omega|^2 = \alpha G - \alpha(\frac{1}{2}V\theta_{0_T} - \frac{1}{2}V_T\theta + \delta_{0_T})\omega \tag{7}$$
$$- \alpha(i\omega_T - i\omega_\theta\theta_{0_T}), \quad \text{where} \quad G = e^{-i(\delta+\frac{V}{2}\theta)}H(\eta).$$

The explicit form of G for the perturbation terms in (7) will be shown later. Next, we expand the solution ω as

$$\omega = \eta_0(\theta) + \alpha\eta_1 + O(\alpha^2), \tag{8}$$

and substitute (8) into (7). The $O(1)$ terms satisfy the unperturbed NLS equation, but at $O(\alpha)$ we obtain

$$i\eta_{1_t} + \eta_{1_{\theta\theta}} - \beta\eta_1 + \eta_0^2\overline{\eta}_1 + 2\eta_0^2\eta_1 = w_1, \quad \text{where} \tag{9}$$
$$w_1 = G_0 - i\eta_{0_T} + i\eta_{0_\theta}\theta_{0_T} - (\frac{1}{2}V\theta_{0_T} - \frac{1}{2}V_T\theta + \delta_{0_T})\eta_0,$$
$$G_0 = e^{-i(\delta+\frac{V}{2}\theta)}H(e^{i(\delta+\frac{V}{2}\theta)}\eta_0), \quad \eta_0 = \sqrt{2}\kappa\,\mathrm{sech}\,\kappa\theta.$$

and $\eta_1|_{t=0} = 0$. By taking $U = (\eta_1, \eta_1^*)^T$ and $\mathcal{H} = (w_1, -w_1^*)^T$, (9) can be represented in matrix form as

$$(i\partial_t + \mathcal{L})U = \mathcal{H}, \quad \text{where} \quad \mathcal{L} = \sigma_3 \begin{pmatrix} \partial_{\theta\theta} - \beta + 2\eta_0^2 & \eta_0^2 \\ \eta_0^2 & \partial_{\theta\theta} - \beta + 2\eta_0^2 \end{pmatrix}, \tag{10}$$
$$\text{and} \quad \sigma_3 = \begin{pmatrix} 1 & 0 \\ 0 & -1 \end{pmatrix}.$$

σ_3 is the Pauli spin matrix. The only remaining problem is to solve (10), which uses the eigenfunctions and eigenvalues of the associated linear operator $\mathcal{L}$. We denote the non-localised (continuous) eigenvectors of $\mathcal{L}$, which are needed for our analysis, by

$$\Psi_1 = e^{-i\xi\theta}\begin{pmatrix} -\kappa^2\,\mathrm{sech}^2\,\kappa\theta \\ (\kappa\tanh\kappa\theta + i\xi)^2 \end{pmatrix}, \Psi_2 = e^{-i\xi\theta}\begin{pmatrix} -(\kappa\tanh\kappa\theta + i\xi)^2 \\ \kappa^2\,\mathrm{sech}^2\,\kappa\theta \end{pmatrix}. \tag{11}$$

The eigenfunctions of $\mathcal{L}^\dagger$, adjoint operator of $\mathcal{L}$, are also needed. These adjoint eigenfunctions are determined by $w^\dagger = (-a^*, b^*)^T$, where $w = (a, b)^T$ is a eigenfunction of $\mathcal{L}$. Note that the eigenfunctions (11) are similar to those related to the linearization problem of the Hirota equation [9]. Lastly, the product

$$\langle f(\theta), g(\theta)\rangle = \int_{-\infty}^{\infty} f(\theta)^T g(\theta) d\theta, \tag{12}$$

needs to be defined. Note, that if g is replaced by its complex conjugate in the integral, then (12) is an inner product, but for soliton perturbation theory, the product (12) need not be positive definite, see Yang [16] or Zhu and Yang [17]. The products in (12) are

real quantities. Suppressing the secular terms gives the first-order solitary wave solution of (10) as,

$$\eta_1 = \frac{1}{5760}\int_{-\infty}^{\infty}[g^+(t;\xi)\Psi_1 + g^-(t;\xi)\Psi_2]d\xi, \quad \text{where} \quad \vartheta = \xi^2 + \kappa^2, \tag{13}$$
$$g^{\pm}(t;\xi) = \pm\frac{M^{\pm}(\xi)}{\vartheta}(1 - e^{\pm i\vartheta t}), \quad M^+(\xi) = \frac{18}{\sqrt{2}\pi\vartheta^2}\langle\mathcal{H}, \Psi_1^{\dagger}\rangle,$$
$$M^-(\xi) = -\frac{18}{\sqrt{2}\pi\vartheta^2}\langle\mathcal{H}, \Psi_2^{\dagger}\rangle.$$

3.2. The first-order perturbation solution

To study the effect of the perturbation terms in (4) on a NLS soliton envelope, we solve (10). The term G_0, which forms part of the first-order forcing term (in (9)), has the form

$$G_0 = H(\eta_0) + iV(-c_2 + c_3 + c_5)\eta_0^2\eta_{0_\theta} + \frac{1}{4}V^2(-c_2 - c_3 + c_4 - c_5)\eta_0^3 \tag{14}$$
$$+ \frac{1}{16}V^4c_6\eta_0 - \frac{1}{2}iV^3c_6\eta_{0_\theta} - \frac{3}{2}V^2c_6\eta_{0_{\theta\theta}} + 2iVc_6\eta_{0_{\theta\theta\theta}}.$$

Substituting (14) into the forcing term (9) and applying the residue theorem to $M^{\pm}$, yields their explicit forms

$$M^{\pm}(\xi) = (a_4\xi^4 \pm a_3\xi^3 + a_2\xi^2 \pm a_1\xi + a_0)\,\mathrm{sech}(b_1\xi), \quad \text{where} \quad b_1 = \frac{\pi}{2\kappa}. \tag{15}$$

So (13) becomes

$$\eta_1(\theta,t) = \frac{1}{5760}\int_{-\infty}^{\infty}\frac{e^{-i\xi\theta}}{\vartheta} \times [M^-(\xi)(1 - e^{-i\vartheta t})(\kappa\tanh\kappa\theta + i\xi)^2 \tag{16}$$
$$- \kappa^2 M^+(\xi)(1 - e^{i\vartheta t})\,\mathrm{sech}^2\,\kappa\theta]d\xi,$$

which is an integral expression for the first-order correction to the solitary wave profile. As the integral expression for η_1 contains no singular points, the Riemann-Lebesgue theorem implies that the shelf $\eta_1 \to 0$, as $t \to \infty$. Hence an asymptotic higher-order NLS solitary wave, valid to $\mathrm{O}(\alpha)$, exists for all values of the higher-order coefficients, as there is no $\mathrm{O}(\alpha)$ shelf at long time.

If the soliton velocity is the same as the phase speed of the linear radiation then resonance can occur, leading to radiation loss from the solitary wave. The linear dispersion relation for (4) is $\omega = k^2 - \alpha c_1 k^4 + \alpha c_{16} k^6$. When $\omega = 0$ the phase velocity of the linear radiation corresponds to the soliton velocity and resonance will occur if $\alpha k^2(c_1 - c_{16}k^2) = 1$. Hence, for general higher-order coefficients, the existence of exact higher-order NLS solitary waves is an open question, as radiation loss may generate a solitary wave tail of $\mathrm{O}(\alpha^2)$.

3.3. Analytical results for the solitary wave tail

The leading order term for the tail, valid for large time, can be determined by the method of stationary phase. To obtain the large time solution we let $\theta = c_p t$ in (16) and consider c_p of either sign. The technique used here is similar to that of Hosieni and Marchant [9] and Pelinovsky and Yang [18], who also obtained large time solutions. The relevant phase of

(16) is $\vartheta_1 = -\xi c_p - \xi^2 - k^2$ and the point of stationary phase, which occurs when $\frac{d\vartheta_1}{d\xi} = 0$, is $\xi_s = -\frac{c_p}{2}$. Using this method gives

$$\eta_1 \sim -\frac{\pi^{\frac{1}{2}}(\kappa - i\frac{c_p}{2})^2 M^-(-\frac{c_p}{2})}{5760 t^{\frac{1}{2}}(\frac{c_p^2}{4} + \kappa^2)} e^{-i(\frac{c_p}{2}t + \frac{\pi}{4})}, \quad |\theta| \gg 1, \quad t \to \infty. \tag{17}$$

The term M^+ makes no contribution to the tail (16) at long times, as $\operatorname{sech}^2 \kappa\theta \approx 0$ for $|\theta| \gg 1$. The expression (17) describes the tail properties along the straight lines $\theta = c_p t$. It can be seen that the amplitude decays like $t^{-1/2}$ along these lines, which is the characteristic decay rate associated with the NLS equation. At a fixed time t, the tail is evaluated by substituting $c_p = \frac{\theta}{t}$ into (17).

[11] found approximate equations for the evolution of a general initial pulse, to the NLS soliton solution. In their work they assumed that the slowly decaying bed of radiation had uniform amplitude and a fixed length. Their uniform amplitude assumption relies on the slope of the bed being much smaller than its amplitude. The expression (17) indicates that the amplitude of the shelf decays like $t^{-\frac{1}{2}}$ while its slope decays like $t^{-\frac{3}{2}}$. Hence the relative slope (compared to its amplitude) of the shelf decays like t^{-1}, much faster than the decay of the shelf itself. The relative slope of the shelf in (17) becomes small for $t \gg 1$, for realistic parameters values. Hence the solution developed here gives insights into the validity of approximate solution techniques, like that of [11].

At large time the tail amplitude is given by the simple expression

$$|\eta_1| \sim \frac{1}{5760}\pi^{\frac{1}{2}} t^{-\frac{1}{2}} |M^-(u)|, \quad |u| \gg 1, \quad t \to \infty, \quad \text{where} \tag{18}$$
$$M^- = (a_2 u^2 - a_1 u + a_0) S, \quad S = \operatorname{sech}(b_1 u), \quad u = -\frac{c_p}{2} = -\frac{\theta}{2t}.$$

Note that $a_3 = a_4 = 0$ for the CN and Taha numerical schemes. Analytical results for the tail amplitude $|\eta_1|$ can be obtained by examining the properties of M^-. The expression M^- is, in general, not symmetric so the left and right tails formed by the evolving soliton are also non-symmetric. This is due the non-symmetry of the phase of the initial soliton. The left and right solitary wave tails are symmetric if $a_1 = 0$. In the special case of a stationary soliton ($a = 0$), the initial phase is symmetric, so the solitary wave tail for the evolving stationary soliton is symmetric as well.

The expression M^- will be examined to classify all the qualitatively different profiles for the tail amplitude $|\eta_1|$. Note that the expression M^- is valid for all u, whilst the tail amplitude is only valid for $|u| \gg 1$.The classification is done by considering various degenerate parameter choices for M^- and is similar to the application of singularity theory to bifurcation problems in combustion theory [19]. The expressions

$$M^-_u = (2a_2 u - a_1) S - b_1 (a_2 u^2 - a_1 u + a_0) ST, \tag{19}$$
$$M^-_{uu} = 2a_2 S - 2b_1 (2a_2 u - a_1) ST + b_1^2 (a_2 u^2 - a_1 u + a_0)(S - 2S^3),$$
$$\text{where } T = \tanh(b_1 u),$$

are used. The hysteresis and zero degenerate points are given by the relations

$$M^-_u = M^-_{uu} = 0, \tag{20}$$
$$M^- = M^-_u = 0, \tag{21}$$

respectively. (20) represents a condition for the occurrence of a hysteresis region in the tail profile while (21) is the condition for the generation of a point of zero amplitude in the tail profile. As the zeros of M^- are governed by a quadratic, the condition (21) simplifies to

$$a_1^2 - 4a_2a_0 = 0. \tag{22}$$

In the special case of $a_1 = 0$ an explicit condition can be found for (20) as the hysteresis point represents a bifurcation from a symmetric tail profile, at $u = 0$. Substituting $a_1 = u = 0$ into (20) gives the condition

$$2a_2 - a_0b_1^2 = 0. \tag{23}$$

The maximum amplitude of a solitary wave tail (the amplitude at its peak) is a measure of the discretization error induced by the numerical scheme. This peak amplitude is given by M^-, where $M_u^- = 0$. To examine the variation of peak amplitude with the discretization ratio β, we take the total derivative of M^-, while keeping the solitary wave parameters a and κ fixed,

$$\frac{dM^-}{d\beta} = M_\beta^- + M_u^- u_\beta. \tag{24}$$

We are interested in choices of β which minimise the peak amplitude hence the condition for local minima is given by

$$M_\beta^- = M_u^- = 0. \tag{25}$$

Note that the function M^- can have multiple peaks so (25) does necessarily represent the global minimum of the peak amplitude. In particular it is possible for the global minimum, wrt to β, to not satisfy $M_\beta^- = 0$, but to occur when M^- has two peaks of the same amplitude.

4. Analytical and numerical results

In this section both analytical and numerical results for the solitary wave tails associated with the CN and Taha numerical schemes are presented and compared. The analytical results are obtained by using the results of soliton perturbation theory, found in §3. The higher-order coefficients, c_j, of the higher-order NLS equation (4), corresponding to the leading-order discretization errors for both schemes, are related to the coefficients a_i of M^-. These relationships are given in Appendix A. Numerical solutions, using the CN and Taha schemes, are also found, for comparison purposes. Also, we note that the NLS equation is invariant under the transformation $(\eta, x, t) = (\kappa\eta^*, \frac{x^*}{\kappa}, \frac{t^*}{\kappa^2})$, so wlog we assume $\kappa = 1$ in all the examples presented below. This choice corresponds to a soliton with amplitude $\sqrt{2}$.

4.1. The Crank-Nicolson numerical scheme

The analytical results for the solitary wave tail depend on the function M^-. For the CN scheme, the coefficients of the quadratic associated with M^- are

$$\begin{aligned} &a_2 = 160\beta^2, \quad a_1 = 480a(\beta^2 + 2a^2), \\ &a_0 = 240\beta^2\kappa^2 + 720a^2\beta^2 + 1440a^4 - 1440\kappa^2a^2. \end{aligned} \tag{26}$$

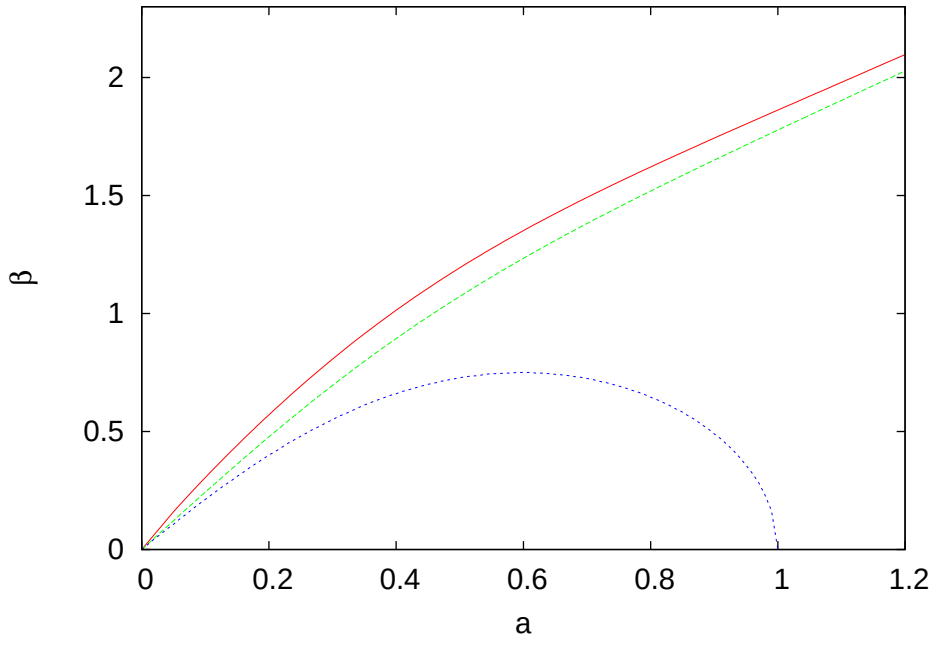

Figure 1. (Colour online) Degenerate hysteresis (red solid curve) and zero curves (green large dashes) and the minimum peak amplitude curve (blue small dashes), for the CN scheme (2), in the a versus β plane.

It can be seen that the solitary wave tail for the CN scheme has the same symmetry property as the NLS soliton; it is invariant under the transformation $(a, \theta) \rightarrow (-a, -\theta)$. This means that both the solitary wave and its tail are reflected about $\theta = 0$ if the sign of the soliton velocity a is changed.

Figure 1 shows the division of the soliton velocity-discretization ratio, (a, β), plane into regions describing the qualitatively different solitary wave tails, for the CN numerical scheme. The degenerate hysteresis (20) and zero curves (21) and the minimum peak amplitude curve are shown. Only solutions for positive velocity a are presented as the solutions are the same for negative a. The degenerate hysteresis and minimum peak amplitude curves are found numerically, while an explicit expression,

$$\beta = (6\kappa^2 a^2 + 2\sqrt{3}a^2(3a^4 + 3\kappa^4 + 2\kappa^2 a^2)^{\frac{1}{2}})(3a^2 + 2\kappa^2)^{-1}, \tag{27}$$

exists for the degenerate zero curve. The expression (27) has the asymptotic relationships $\beta \sim \sqrt{2}a, a \gg 1$ and $\beta \sim \sqrt{6}a, a \ll 1$.

There are three different regions in the plane corresponding to the three qualitatively different kinds of solitary wave tail. Above the degenerate hysteresis curve the tail profile has a single peak and decays monotonically to zero as $\theta \rightarrow \pm\infty$. The peak can occur in the left or right tail, depending on the value of a. For $a = 0$, M^- has a peak, located at $\theta = 0$. As the long time solution for $|\eta_1|$ is not valid for $\theta = 0$, this peak is not numerically realised; the left and right tails, for $|\theta| \gg 1$, undergo monotonic decay. In the region bounded by the degenerate hysteresis and zero curves multiple peaks occur, in the tail profile. In this parameter region the tail amplitude, $|\eta_1|$, has continuous slope. In the region below the degenerate zero curve multiple peaks also occur, but the tail amplitude,

$|\eta_1|$ has discontinuous slope, at the zeros, where $\eta_1 = 0$. Note that this discontinuity occurs in the slope of the amplitude $|\eta|$, not η itself, and the derivative term η_{xx} of the NLS equation is continuous.

The degenerate hysteresis curve has a cusp point, which represents a bifurcation from a symmetric tail profile, at $u = 0$. The cusp point can can be found by solving the equation (23) and $a_1 = 0$. These conditions have the single cusp solution $(a, \beta) = (0, 0)$. Here the bifurcation, from a symmetric profile occurs in a similar way to that seen in [12] (see their figure 1), except that in [12] the cusp point occurs for a finite value of β. For all values of a all three types of solitary wave are possible. For example, at $a = 1$ a solitary wave tail with discontinuous slope occurs for $\beta < 0.560$, a tail with multiple peaks and continuous slope occurs for $\beta \in [0.560, 0.776)$ while for $\beta \geq 0.776$ a tail with a single peak occurs.

A critical aspect of a numerical scheme is its efficiency, namely its ability to calculate accurate solutions at low computational cost. Here the maximum, or peak, amplitude of the solitary wave tail is a useful measure of the discretization error of the numerical scheme. The minimum peak amplitude curve describes the parameter values at which the peak of the solitary wave tail is a minimum, over all values of β. For $a \geq 1$ this minimum peak amplitude occurs in the limit as $\beta \to 0$. In this limit, $\Delta x \to 0$, the discretization error is $\mathrm{O}(\Delta t^2)$. For $a \in (0, 1)$ however, the minimum peak amplitude occurs at a finite value of β. The curve represents optimal choices of the discretization ratio β, for minimising the discretization error in these cases, at the lowest computational cost. For the CN scheme the minimum peak amplitude curve does not satisfy (25). Here the minimal solitary wave tail has two peaks of the same amplitude, and is found by a direct search of the parameter space.

Figures 2 and 3 shows the evolution of a NLS solitary wave using the CN numerical scheme. Shown is the solitary wave tail amplitude, $|\eta_1|$ versus θ, for $t = 50$. The other parameters are $\Delta x = \Delta t = 0.01$ and $a = \beta = 1$. Shown is the analytical tail amplitude (18) and the CN numerical solution (2). For all the numerical solutions considered in this paper, the quantity $\alpha^{-1}|\eta - \eta_0|$ is plotted, where η_0 is the NLS soliton solution (5). This quantity represents the appropriate comparison with the perturbation solution η_1, in the tail regions, away from the solitary wave, located at $\theta = 0$.

For this example $(a, \beta) = (1, 1)$ so the solution is in the region of parameter space corresponding to multiple peaks, where the tail amplitude $|\eta_1|$, has discontinuous slope. It can be seen that the perturbation and numerical solutions are the same to graphical accuracy, except near $\theta = 0$, where the soliton is located. The tail profile has both peaks and zeros occurring. Solving the quadratic associated with M^- gives the analytical location of the zeros as $c_p = -16.55$ and -1.45. Solving $M_u = 0$ gives the location of two of the peaks as $c_p = -2.650$ and 0.908, with the third occurring for $c_p < -16.55$. Hence the left tail has two zeros and two peaks while the right tail has no zero and one peak. At $t = 50$ the analytical location of the zeros are $\theta = -822.5$ and -72.50 and the peaks are $\theta = -132.5$ and 45.5. The amplitudes of the peaks are $|\eta_1| = 7.13 \times 10^{-3}$ and 5.66×10^{-2}, respectively. Numerically the location of the zero closest to the soliton is $\theta = -74.0$, while the peaks are located at $\theta = -133.15$ and 47.1, with amplitudes 7.15×10^{-3} and 5.77×10^{-2}, respectively. The variation between the analytical and numerical peak and zero locations

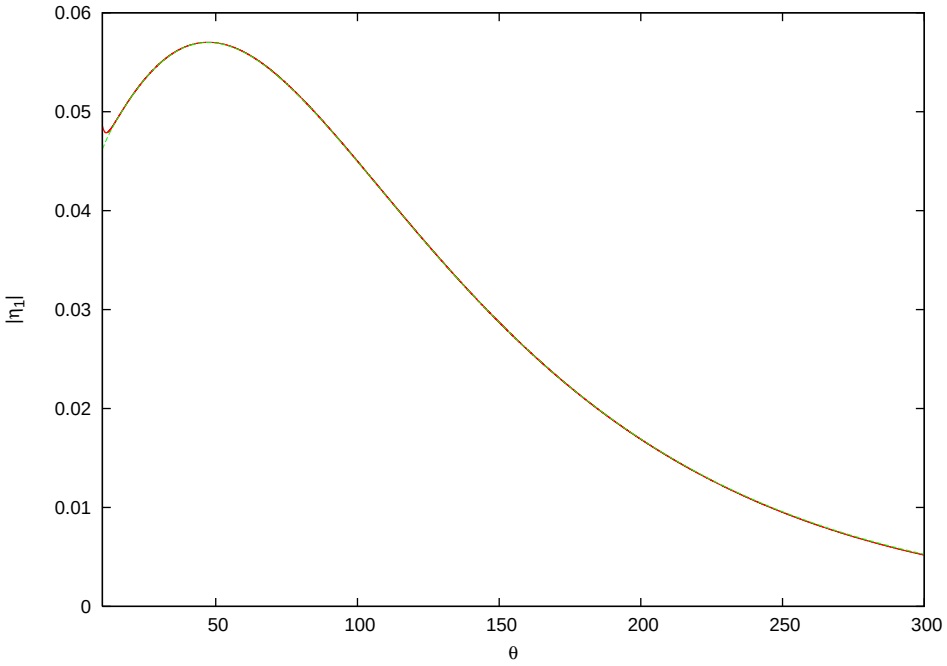

Figure 2. (Colour online) The amplitude of the right solitary wave tail, $|\eta_1|$ versus θ, at $t = 50$, for the CN scheme (2). The parameters are $\Delta x = \Delta t = 0.01$, $\beta = a = 1$. Shown are the analytical (red solid curve) numerical (green dashed curve) solutions.

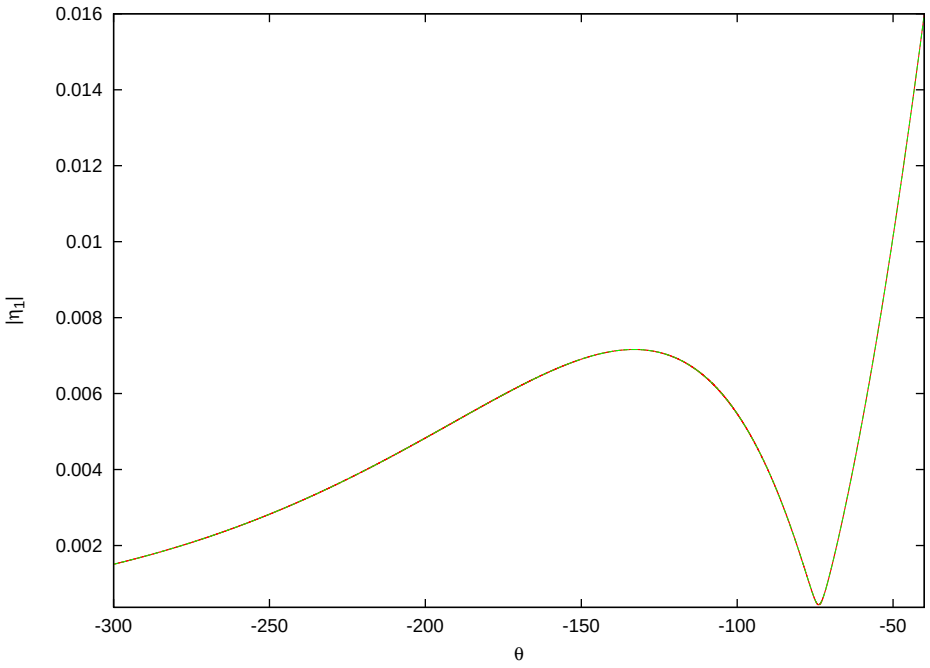

Figure 3. (Colour online) The amplitude of the left solitary wave tail, $|\eta_1|$ versus θ, at $t = 50$, for the CN scheme (2). The parameters are $\Delta x = \Delta t = 0.01$, $\beta = a = 1$. Shown are the analytical (red solid curve) numerical (green dashed curve) solutions.

is less than 2% of the distance the soliton has travelled, at $t = 50$. The analytical and numerical peak amplitudes also differ by less than 2%. Due to the near exponential decay

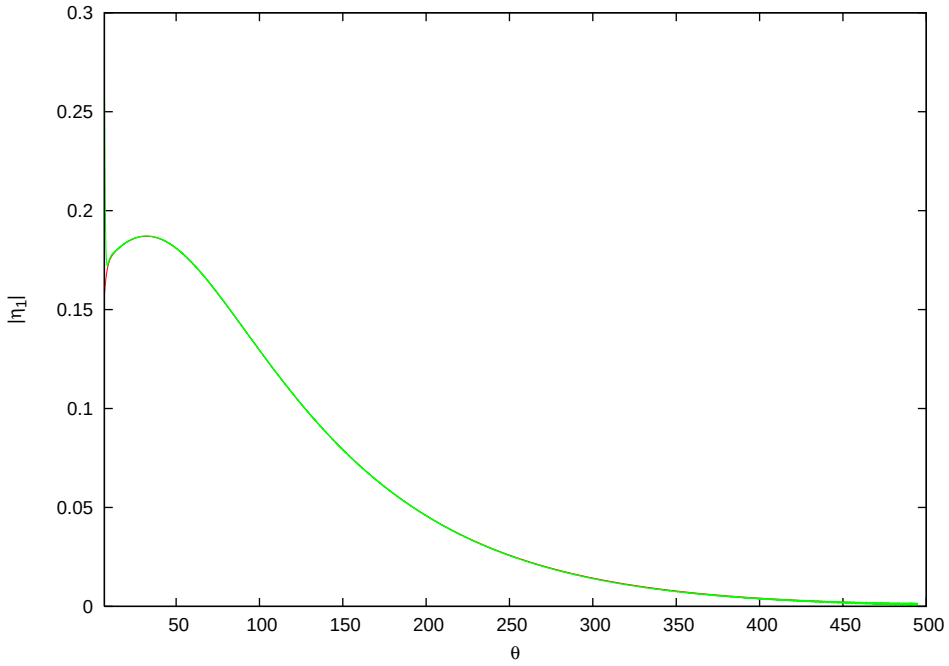

Figure 4. (Colour online) The amplitude of the right solitary wave tail, $|\eta_1|$ versus θ, at $t = 50$, for the CN scheme (2). The parameters are $\Delta x = 0.02$, $\Delta t = 0.01$, $\beta = 2$ and $a = 1$. Shown are the analytical (red solid curve) numerical (green dashed curve) solutions.

of the shelf for large $|\theta|$, no numerical comparisons are made for the zero at $\theta = -822.5$ and the peak beyond this zero. This is because $|\eta_1| < 10^{-7}$ in this region of the tail, where neglected $O(\alpha^2)$ discretization errors, and also round-off errors, become significant.

Figures 4 and 5 shows the evolution of a NLS solitary wave using the CN numerical scheme. Shown is the solitary wave tail amplitude, $|\eta_1|$ versus θ, for $t = 50$. The other parameters are $\Delta x = 0.02$, $\Delta t = 0.01$, $\beta = 2$ and $a = 1$. Shown is the analytical tail amplitude (18) and the CN numerical solution (2). For this example $(a, \beta) = (1, 2)$ so the solution is in the region of parameter space corresponding to a single peak for the solitary wave tail. It can be seen that the perturbation and numerical solutions are the same to graphical accuracy, except near $\theta = 0$, where the soliton is located. Solving $M_u = 0$ gives the analytical location of the peak as $c_p = 0.596$. Hence the left tail is monotonic while the right tail has a single peak. At $t = 50$ the analytical location of the peak is $\theta = 29.8$ whilst its amplitudes is $|\eta_1| = 0.186$. Numerically, the peak is located at $\theta = 30.2$ and its amplitude is 0.187. The variation between the analytical and numerical peak locations is less than 1% of the distance the soliton has travelled, at $t = 50$. The analytical and numerical peak amplitudes differ by less than 0.5%.

4.2. The Taha numerical scheme

For the Taha numerical scheme, the coefficients of the quadratic associated with M^- are

$$a_2 = 40\beta^2 - \frac{460}{3}\beta a + \frac{1400}{3}a^2, \quad a_1 = 20a(83a^2 - 35\kappa^2 - 28\beta a), \tag{28}$$

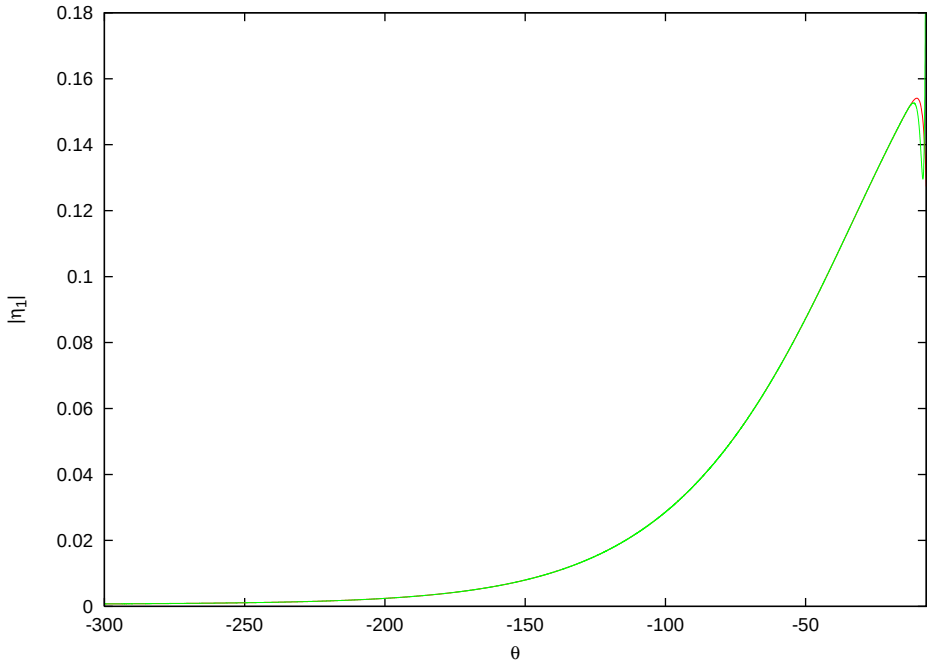

Figure 5. (Colour online) The amplitude of the left solitary wave tail, $|\eta_1|$ versus θ, at $t = 50$, for the CN scheme (2). The parameters are $\Delta x = 0.02$, $\Delta t = 0.01$, $\beta = 2$ and $a = 1$. Shown are the analytical (red solid curve) numerical (green dashed curve) solutions.

$$a_0 = 540\beta\kappa^2 a + 1440a^4 - 1440\kappa^2 a^2 - 120\beta^2\kappa^2.$$

Unlike the CN tail the Taha tail does not have the same symmetry property as the NLS soliton, as changing the sign of the velocity a leads to a different solitary wave tail.

Figure 6 shows the division of the (a, β) plane into regions describing the qualitatively different solitary wave tails, for the Taha numerical scheme. The degenerate hysteresis (20) and zero curves (21) and the minimum peak amplitude curve are shown. The curves are all found numerically. Again there are three qualitatively different kinds of solitary wave tail. To the right of the degenerate hysteresis curve the tail profile has a single peak and decays monotonically to zero as $\theta \to \pm\infty$. In the region bounded by the degenerate hysteresis and lower zero curves multiple peaks occur, in the tail profile. In this parameter region the tail amplitude, $|\eta_1|$, has continuous slope. In the region to the left of the degenerate zero curve multiple peaks also occur, but the tail amplitude, $|\eta_1|$ has discontinuous slope. For $a < 0.805$ only one type of tail (with multiple peaks and discontinuous slope) occurs, while for $a \geq 0.805$ all three types of solitary wave tail are possible depending on the value of β. For example, at $a = 1$ a solitary wave tail with discontinuous slope occurs for $\beta < 0.56$ and $\beta > 3.27$, a tail with multiple peaks and continuous slope occurs for $\beta \in [0.56, 0.776)$ and $\beta \in (3.06, 3.27]$ while for $\beta \in [0.776, 3.06]$ a tail with a single peak occurs.

The cusp point for the degenerate hysteresis curve occurs at $(a, \beta) = (0.905, 1.30)$. Here the bifurcation, from a symmetric profile occurs at a non-zero value of a, this is in contrast to [12] and the CN scheme, for which the cusp point occurred for a stationary soliton, with $a = 0$. There are no cusp points or degenerate hysteresis curves in the plane

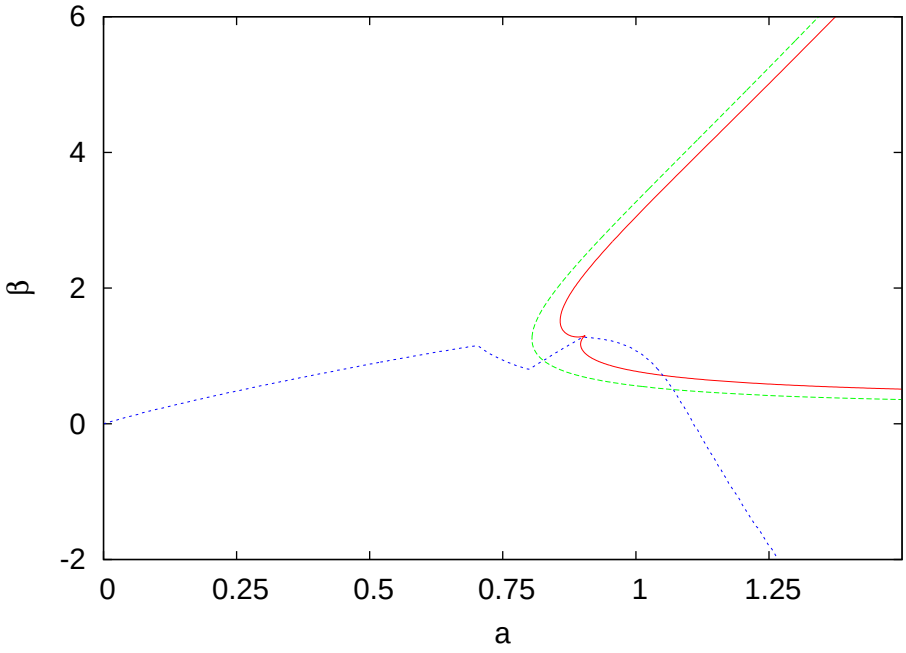

Figure 6. (Colour online) Degenerate hysteresis (red solid curve) and zero curves (green large dashes) and the minimum peak amplitude curve (blue small dashes), for the Taha scheme (3), in the a versus β plane.

for negative soliton velocities a. For the degenerate zero curve this non-symmetry can be shown analytically. The degenerate zero curve is given by the quartic equation, for β,

$$48\kappa^2\beta^4 - 400a\kappa^2\beta^3 + \beta^2(208a^4 + 1964a^2k^2) - \beta(2440a^5 + 2768a^3k^2) + 169a^6 + 910a^4k^2 + 1225a^2k^4 = 0. \quad (29)$$

This equation (29) does not have any positive roots for negative a (all the terms are positive in this case), so there are no degenerate zero curves for $a < 0$.

The peak amplitude curve describes parameter values at which the peak of the solitary wave tail has minimum amplitude, over all values of β. The minimum peak amplitude occurs at finite β for $a \in (0, 1.11)$ and for $a < -1.11$. For other values of a the minimum peak amplitude occurs at $\beta = 0$. Note that, for convenience, the peak amplitude curve is displayed for positive a only but for all values of β. The peak amplitude curve is anti-symmetric wrt a hence the portion of the curve, for $a > 1.11$, with negative (and non-physical) values of β corresponds to the curve for $a < -1.11$ (and with positive β). For the Taha scheme (25) is satisfied for all of the minimum peak amplitude curve except a small portion of the curve between $0.701 < a < 0.900$. In this region the solitary wave tail of minimum amplitude has two equal peaks, which is true of the miminal CN waves also.

The figure shows that properties of the Taha tail are different for left and right moving solitary waves, illustrating an unusual non-symmetry of the Taha scheme, which does not occur for the CN scheme. For the CN scheme the three types of solitary wave tail occur for all values of a, while for the Taha scheme three types only occur for $a > 0.805$ and one

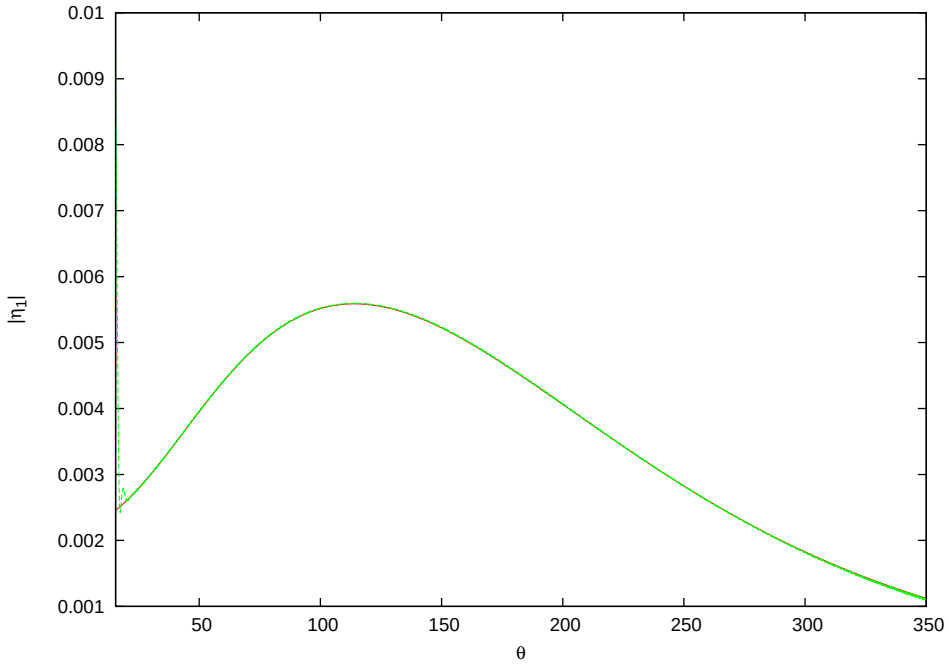

Figure 7. (Colour online) The amplitude of the right solitary wave tail, $|\eta_1|$ versus θ, at $t = 50$, for the Taha scheme (3). The parameters are $\Delta x = \Delta t = 0.01$, $\beta = 1$ and $a = 0.85$. Shown are the analytical (red solid curve) numerical (green dashed curve) solutions.

type otherwise.

Figure 7 and 8 shows the evolution of a NLS solitary wave using the Taha numerical scheme. Shown is the solitary wave tail amplitude, $|\eta_1|$ versus θ, for $t = 50$. The other parameters are $\Delta x = \Delta t = 0.01$, $\beta = 1$, $a = 0.85$ and $\kappa = 1$. Shown is the analytical tail amplitude (18) and the numerical solution of the Taha scheme (3). For this example $(a, \beta) = (0.85, 1)$ so the solution is in the region of parameter space corresponding to multiple peaks, where the tail amplitude $|\eta_1|$, has continuous slope. It can be seen that the perturbation and numerical solutions are the same to graphical accuracy, except near $\theta = 0$, where the soliton is located. The tail profile has a peak in the left and right tails. Solving $M_u = 0$ gives the location of the peaks as $c_p = -2.40$ and 2.27. At $t = 50$ the analytical location of the peaks are $\theta = -120.0$ and 113.5 whilst the amplitudes are $|\eta_1| = 4.93 \times 10^{-3}$ and 5.56×10^{-3}, respectively. Numerically, the peaks are located at $\theta = -120.2$ and 113.2 and their amplitudes are 4.95×10^{-3} and 5.59×10^{-3}, respectively. The variation between the analytical and numerical peak locations, compared to the distance travelled by the soliton, is less than 0.5%, while the analytical and numerical peak amplitudes differ by less than 0.5%.

5. Conclusion

In this paper, soliton perturbation theory is used to study NLS solitary wave tails, induced by the discretization errors of the CN and Taha numerical schemes. The analytical form for the solitary wave tail proves useful for investigating a range of qualitatively different

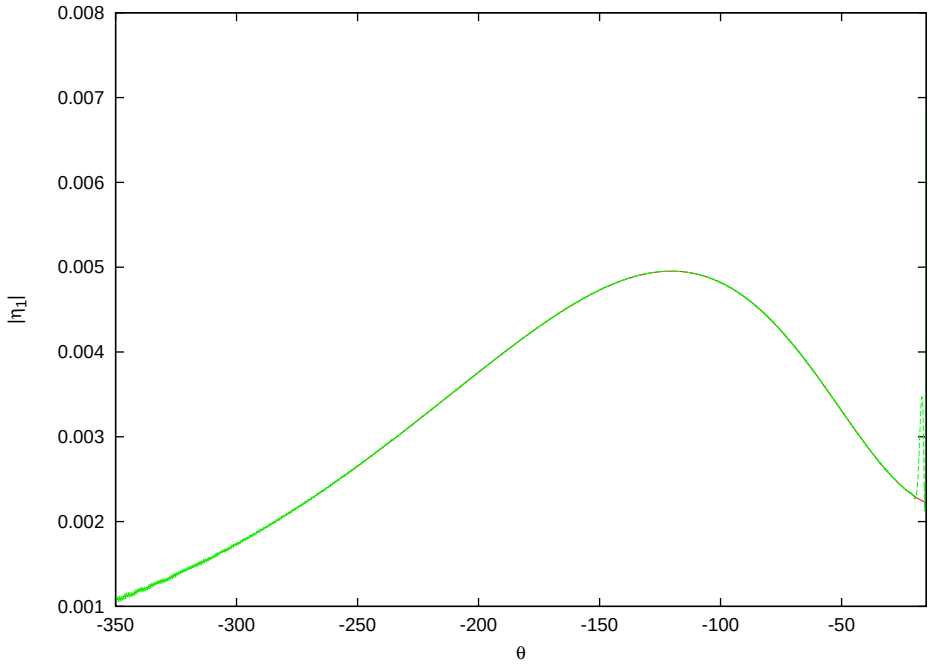

Figure 8. (Colour online) The amplitude of the left solitary wave tail, $|\eta_1|$ versus θ, at $t = 50$, for the Taha scheme (3). The parameters are $\Delta x = \Delta t = 0.01$, $\beta = 1$ and $a = 0.85$. Shown are the analytical (red solid curve) numerical (green dashed curve) solutions.

tail properties and for examining how the discretization parameters affect the amplitude of the solitary wave tail. The results show that three types of solitary wave tails occur, depending on the parameter values used. It was also found that the amplitude of the solitary wave tail is minimized for a finite discretization ratio, with optimal choices of the discretization ratio identified.

The analytical solution also illustrates the symmetry properties of the numerical schemes. The CN scheme is symmetric as the same tail is obtained for both left and right moving solitary waves but the Taha scheme is not. The results show that a much richer variety of solitary wave tails occur for right moving solitary wave tails, than for left moving ones, for the Taha scheme. The Taha numerical scheme preserves integrability (so numerical solitary wave collisions are elastic) and is computationally efficient. However, this study illustrates that the Taha scheme is not symmetric. Hence the advantages of the Taha scheme, that it is integrable, must be balanced against its unusual, and non-physical, symmetry properties. On the other hand the CN numerical scheme preserves symmetry but is not integrable and is not as computationally efficient as the Taha scheme. Therefore it is not clear cut what numerical scheme for the NLS equation is best in practice; the Taha scheme is probably preferable but the user should exercise caution regarding any non-physical aspects of the solution. The analysis presented here only applies to a single NLS soliton and not to interacting NLS solitons (which can have different velocities) or a more general initial condition. However, some of the insights from this study are still useful when considering these more general scenarios.

The exact form of the solitary wave tail, found here, also provides insights into the

validity of approximate solution methods describing NLS solitary wave evolution. The method of [11] assumes that the shelf has uniform amplitude and the perturbation solution found here indicates that the relative slope of waves on the shelf decays like t^{-1}, a faster decay rate than that of the shelf itself. So the exact solution provides a timescale for which the flat shelf approximation, of [11], becomes valid.

In conclusion, it is found that soliton perturbation theory is a highly useful tool, for examining the behaviour of numerical schemes for the NLS equation. Future work could examine the behaviour of numerical schemes for other integrable equations, or examine the evolution of dark solitary waves.

Acknowledgement: The authors would like to thank two anonymous referees for their useful comments. The research of SMH is under the grant p/2738, of Vali-E-Asr university. Also SMH would like to thank his wife S. Zahedi Nejad for her patience and encouragement.

Appendix A. Relations for the coefficients of M^-

The dependence of the coefficients of the function M^- in (15) are related to the higher-order coefficients of the perturbed NLS equation (4) by

$$
\begin{aligned}
a_4 &= 3(24c_2 - 2c_3 - c_4 - c_5 - 2c_6 + 2c_7 + 6c_8 + 6c_9 + 4c_{10} + c_{11} \\
&+ 6c_{12} - c_{13} + 2c_{14} + 4c_{15} - 720c_{16} + 24c_{17}), \\
a_3 &= 16(6c_{22} - c_{23} - c_{24} + 2c_{25} + 2c_{26} + 2c_{27} + 6c_{28}) + 16a(2c_6 \\
&- 24c_2 - 2c_3 + 2c_5 + 2c_7 + 12c_9 + 8c_{10} - 2c_{13} + 2c_{14} - 720c_{16} + 24c_{17}), \\
a_2 &= 2[960c_1 - 80c_{18} - 40c_{19} - 80c_{20} - 40c_{21} + (480c_2 - 40c_3 + 40c_4 \\
&- 40c_5 - 40c_6 - 40c_7 - 120c_8 + 360c_9 + 320c_{10} - 120c_{12} - 40c_{13} \\
&- 40c_{14} - 14400c_{16} + 480c_{17})a^2 + (240c_{22} + 40c_{23} - 40c_{24} + 160c_{25} - 240c_{28})a \\
&+ (424c_2 - 62c_3 - 11c_4 - 11c_5 - 62c_6 - 18c_7 + 26c_8 + 26c_9 + 44c_{10} \\
&+ 51c_{11} + 26c_{12} - 11c_{13} - 18c_{14} + 44c_{15} - 3120c_{16} + 424c_{17})\kappa^2], \\
a_1 &= 48[(120c_1 + 10c_{18} - 10c_{19} - 10c_{20})a + (13c_{22} - 3c_{23} - 3c_{24} + c_{25} + c_{26} \\
&+ c_{27} + 13c_{28})\kappa^2 + (10c_8 - 20c_2 - 10c_7 + 20c_9 + 20c_{10} - 10c_{12} - 600c_{16} + 20c_{17})a^3 \\
&+ (15c_{22} + 15c_{25} - 5c_{26} - 5c_{27} + 15c_{28})a^2 + (6c_6 - 52c_2 - 6c_3 + 6c_5 - 4c_7 \\
&+ 10c_8 + 16c_9 + 4c_{10} - 10c_{12} - 6c_{13} + 6c_{14} - 360c_{16} + 52c_{17})a\kappa^2], \\
a_0 &= (2880c_1 - 720c_{18} - 720c_{20})\kappa^2 + (720c_{22} + 720c_{25} - 720c_{26} + 720c_{27} \\
&- 720c_{28})a^3 + (8640c_1 - 720c_{18} - 720c_{19} - 720c_{20} + 720c_{21})a^2 + (2520c_2 - 630c_3 \\
&+ 45c_4 + 45c_5 - 630c_6 - 90c_7 - 270c_8 - 270c_9 + 540c_{10} + 675c_{11} - 270c_{12} \\
&+ 45c_{13} - 90c_{14} - 12240c_{16} + 540c_{15} + 2520c_{17})\kappa^4 + (2160c_{22} + 720c_{23} \\
&- 720c_{24} + 720c_{25} - 720c_{26} + 720c_{27} - 2160c_{28})a\kappa^2 + (4320c_2 - 720c_3 \\
&+ 720c_4 - 720c_5 - 720c_6 - 720c_7 - 2160c_8 + 2160c_9 + 1440c_{10} - 2160c_{12} \\
&- 720c_{13} + 720c_{14} + 1440c_{15} - 43200c_{16} + 4320c_{17})a^2\kappa^2 + (720c_2 - 720c_7
\end{aligned}
$$

$$- 720c_8 + 720c_9 + 720c_{10} - 720c_{12} + 720c_{14} + 720c_{15} - 21600c_{16} + 720c_{17})a^4.$$

References

[1] T. R. Taha. Numerical simulation of the nonlinear Schrödinger equation. *Math. Comp. Simul.*:32, 309–312:1990.

[2] T.B. Benjamin and J. F. Feir. The disintegration of wavetrains on deep water. *J. Fluid Mech.*:27, 417–430:1967.

[3] D. H. Peregrine. Water waves and their development in space and time. *Proc. Roy. Soc. Lond. A*:400, 1–18:1985.

[4] H. C. Yuen and B. M. Lake. Nonlinear dynamics of deep-water gravity waves. *Adv. Appl. Mech.*:22, 67–229:1982.

[5] A. Hasegawa and F.D. Tappert. Transmission of stationary nonlinear optical pulses in dispersive dielectric fibres. I. Anomalous dispersion. *Appl. Phys. Lett.*:23, 142–144:1973.

[6] S. Wabnitz, Y. Kodama, and A. B. Aceves. Control of optical soliton interactions. *Opt. Fibr. Tech.*:1, 187–217:1995.

[7] J. Yang. Complete eigenfunctions of linearized integrable equation expanded around a soliton solution. *J. Math. Phys.*:41, 6614–6638:2000.

[8] X-J. Chen and J Yang. Direct perturbation theory for solitons of the derivative nonlinear Schrödinger equation and the modified nonlinear Schrödinger equation. *Phys. Rev. E*:65, 066608:2002.

[9] S.M. Hoseini and T. R. Marchant. Solitary wave interaction and evolution for a higher-order Hirota equation. *Wave Motion*:44, 92–106:2006.

[10] S.M. Hoseini and T. R. Marchant. Solitary wave interaction for a higher-order nonlinear Schrödinger equation. *IMA J. Appl. Math.*:72, 206–222:2007.

[11] W.L. Kath and N.F. Smyth. Soliton evolution and radiation loss for the nonlinear Schrödinger equation. *Phys. Rev. E*:51, 1484–1492:1995.

[12] S.M. Hoseini and T. R. Marchant. Evolution of solitary waves for a perturbed nonlinear Schrödinger equation. *Appl. Math. Comp.*:216, 3642–3651:2010.

[13] T. R. Taha and M. J. Ablowitz. Analytical and numerical aspects of certain nonlinear evolution equations. II. Numerical, nonlinear Schrödinger equation. *J. Comp. Phys.*:55, 231–253:1984.

[14] S. D. Conte and C. deBoor. *Elementary numerical analysis.* McGraw-Hill:New York:1972.

[15] J. Yang and D. J. Kaup. Stability and evolution of solitary waves in perturbed generalized nonlinear Schrödinger equations. *SIAM J. Appl. Math.*:60, 967–989:2000.

[16] J. Yang. Stable embedded solitons. *Phy. Rev. Lett.*:91, 143903:2003.

[17] Y. Zhu and J. Yang. Universal fractal structure in the weak interaction of solitary waves in generalized nonlinear Schrödinger equations. *Phy. Rev. E.*:75, 036605:2007.

[18] D. E. Pelinovsky and J. Yang. A normal form for nonlinear resonace of embedded solitons. *Proc. Roy. Soc. Lond. A*:458, 1469–1497:2002.

[19] M. Golubitsky and D. G. Schaeffer. *Singularites and groups in bifurcation theory.* Springer-Verlag:New York:1985.